Weierstraß-Institut
für Angewandte Analysis und Stochastik

Leibniz-Institut im Forschungsverbund Berlin e. V.

Preprint ISSN 2198-5855

Impact of the capture time on the series resistance of quantum-well diode lasers

Anisuzzaman Boni[1], Hans-Jürgen Wünsche[1,2], Hans Wenzel[1], Paul Crump[1]

submitted: July 1, 2020

[1] Ferdinand-Braun-Institut
Leibniz Institut für Höchstfrequenztechnik
Gustav-Kirchhoff-Straße 4
12489 Berlin
Germany
E-Mail: anisuzzaman.boni@fbh-berlin.de
hans-juergen.wuensche@fbh-berlin.de
hans.wenzel@fbh-berlin.de
Paul.Crump@fbh-berlin.de

[2] Weierstrass Institute
Mohrenstr. 39
10117 Berlin
Germany
E-Mail: hans-juergen.wuensche@wias-berlin.de

No. 2735
Berlin 2020

2010 *Mathematics Subject Classification.* 78A60.

2010 *Physics and Astronomy Classification Scheme.* 42.55.Px, 42.65.Sf, 73.21.Fg, 73.43.Cd.

Key words and phrases. Semiconductor laser, capture–escape, simulation, experiment.

We thank TRUMPF Laser GmbH and the Leibniz-Association within the Cryolaser project for supporting this work. Helpful discussions with Thomas Koprucki and Markus Kantner on numerical aspects are acknowledged as well.

Edited by
Weierstraß-Institut für Angewandte Analysis und Stochastik (WIAS)
Leibniz-Institut im Forschungsverbund Berlin e. V.
Mohrenstraße 39
10117 Berlin
Germany

Fax: +49 30 20372-303
E-Mail: preprint@wias-berlin.de
World Wide Web: http://www.wias-berlin.de/

Impact of the capture time on the series resistance of quantum-well diode lasers

Anisuzzaman Boni, Hans-Jürgen Wünsche, Hans Wenzel, Paul Crump

Abstract

Electrons and holes injected into a semiconductor heterostructure containing quantum wells are captured with a finite time. We show theoretically that this very fact can cause a considerable excess contribution to the series resistivity and this is one of the main limiting factors to higher efficiency for GaAs based high-power lasers. The theory combines a standard microscopic-based model for the capture-escape processes in the quantum well with a drift-diffusion description of current flow outside the quantum well. Simulations of five GaAs-based devices differing in their Al-content reveal the root-cause of the unexpected and until now unexplained increase of the series resistance with decreasing heat sink temperature measured recently. The finite capture time results in resistances in excess of the bulk layer resistances (decreasing with increasing temperature) from 1 mΩ up to 30 mΩ in good agreement with experiment.

1 Introduction

GaAs-based broad area lasers are the most efficient high-power light source and are widely used directly as well as pump sources for solid state lasers. Sustained experimental and theoretical efforts are needed to increase their power and efficiency. Reducing the operating temperature of diode lasers increases optical output power and efficiency, as shown in [3]. The reason for the improved performance with reduced temperature is the enhancement of modal gain and differential internal efficiency [6]. However, lowest series resistance R_s is also needed to maintain high efficiency at high bias. R_s increases sharply with lower operating temperature [6, 7, 8]. This behaviour is in contrast to estimations of the bulk layer resistances and drift-diffusion based simulations [13], which predict that resistance should decrease with lower operating temperature T due to increased mobility and stable carrier densities in the range studied ($200 - 300$ K). More specific, the increase of R_s is found to be roughly proportional to the relative barrier height $\Delta E/kT$ where kT is the thermal energy and ΔE is the energetic barrier for the evaporation of electrons bound in the quantum well (QW) into unbound states and consistent across various structures and operating wavelength. But no detailed studies have been conducted and the origin of the excess R_s is still unknown.

In this paper, we study theoretically the capture-escape mechanism of a quantum well as a possible source of the excess resistance. Our hypothesis is that the capture of particles with a finite transition probability causes an excess series resistance. Capture-escape limitations of carrier collection into QWs are long known [17, 19]. Their consequences have been investigated mostly in the context of modulation properties [14, 20, 4, 5] and power-current characteristics [1]. The impact of capture-escape on the series resistance has not been addressed yet.

The article is organized as follows. We first discuss the theoretical model underlying the simulations. Then we present details of laser structure and simulation parameters, followed by the results section

DOI 10.20347/WIAS.PREPRINT.2735 Berlin 2020

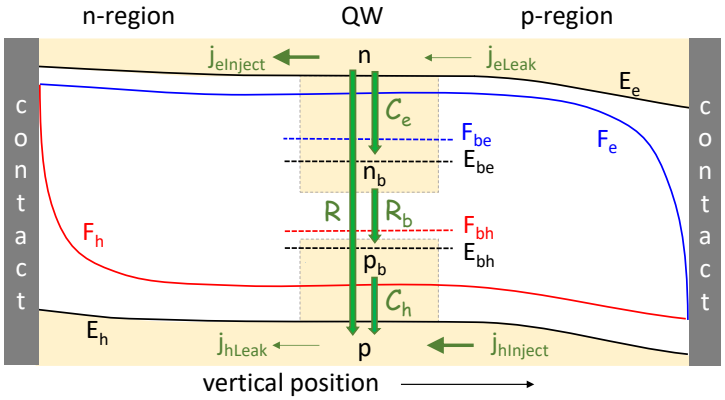

Figure 1: Sketch of the three regions of the 1D laser model. Heterojunctions are not drawn for clarity. Black: band edges. Blue and red: quasi Fermi energies of electrons and holes, respectively. Green: electrical current densities at the border of the QW as well as capture and recombination densities in the QW. Further explanations in the text.

containing three parts. First, the impact of capture time on power-current and voltage-current characteristics will be analysed. Second and third, the dependence of differential resistance on temperature as well as barrier height and effective barrier height, respectively, will be studied. Finally, we compare the simulation results for finite and zero capture times with experimental results.

2 Theoretical approach

We consider broad area single quantum well (SQW) diode lasers in a stationary state above threshold. The lasing region is assumed to be laterally homogeneous. Vertically, it consists of a p-doped region, a n-doped region, and a QW in between as illustrated in Fig. 1. Of course, this sketch is not to scale. The width d of the QW measures only few nm. The doped regions several microns wide are sophisticated multi-heterostructures, which are not resolved in the sketch for clarity.

For simplicity, only one bound and one extended state are considered in the quantum well. The wave functions of the bound states are vertically confined to the QW but laterally unconfined. The wave functions of the extended states are unconfined in all three dimensions. The energy spectra of both types are continuous with edges at $E_{\mathrm{b}\nu}$ and E_ν for bound and extended states, respectively. Here and in the following, the index ν distinguishes between electrons ($\nu = e$) and holes ($\nu = h$). Quantities belonging to bound states are indicated by an additional index b. Out of the QW there are only extended states. We name particles occupying extended states as free particles in contrast to bound particles occupying bound states. The flow of free particles through the doped regions will be described by classical drift-diffusion equations. Balance equations are used for particles in the QW. Exchange between the QW and its outer regions is quantified by injection current densities $j_{\nu\mathrm{Inject}}$ of majorities and leakage current densities $j_{\nu\mathrm{Leak}}$ of minorities.

2.1 Balance equations for the QW

We do not resolve spatial variations in the QW but use quantities averaged over its width d. Free electrons are injected from from the n-doped region (left) with current density j_{eInject}. The injected electrons partly recombine with net rate R, partly are captured with net rate C_{e} into bound states, and

partly leave the QW region on the opposite side with a hopefully small leakage current density j_{eLeak}. The equivalent considerations hold for the holes injected from the p-doped region (right). The captured electrons and holes recombine with net rate R_{b} including stimulated recombination. Obviously, the following balances must hold

$$\begin{aligned} edR_{\mathsf{b}} = edC_{\mathsf{e}} &= |j_{\mathsf{eInject}} - j_{\mathsf{eLeak}}| - edR \\ &= edC_{\mathsf{h}} = |j_{\mathsf{hInject}} - j_{\mathsf{hLeak}}| - edR. \end{aligned} \tag{1}$$

Further requirements in the QW are charge neutrality and the lasing condition,

$$(n + n_{\mathsf{b}}) - (p + p_{\mathsf{b}}) = N_D - N_A \quad \text{and} \tag{2}$$

$$\Gamma g(n_{\mathsf{b}}, p_{\mathsf{b}}) = \alpha, \tag{3}$$

respectively. Here, n, n_{b} and p, p_{b} are the free and bound electron and hole densities, respectively, and N_D and N_A are the fully ionized donor and acceptor densities. Γ denotes the optical QW confinement factor, g the material gain and α the optical losses. To exploit these equations we shall now specify step by step their ingredients.

The microscopic calculation of net capture rates is rather involved [2, 11, 12]. Instead, we use the simple model expressions

$$\begin{aligned} C_{\mathsf{e}} &= \frac{n}{\tau_{\mathsf{e}}} \left(1 - \exp\left[\frac{F_{\mathsf{be}} - F_{\mathsf{e}}}{kT}\right]\right) \\ C_{\mathsf{h}} &= \frac{p}{\tau_{\mathsf{h}}} \left(1 - \exp\left[\frac{F_{\mathsf{h}} - F_{\mathsf{b}h}}{kT}\right]\right) \end{aligned} \tag{4}$$

with the free carrier densities in Boltzmann approximation,

$$\begin{aligned} n &= N_c \exp[\eta_{\mathsf{e}}], \qquad \eta_{\mathsf{e}} = \frac{F_{\mathsf{e}} - E_{\mathsf{e}}}{kT}, \\ p &= N_v \exp[\eta_{\mathsf{h}}], \qquad \eta_{\mathsf{h}} = -\frac{F_{\mathsf{h}} - E_{\mathsf{h}}}{kT}. \end{aligned} \tag{5}$$

$F_{\mathsf{b}\nu}$, F_ν and $E_\nu = E_{c/v} - e\varphi$ with the electrostatic potential φ denote quasi Fermi energies of bound and free particles, and the local band edge energies, respectively. The first term in the net rates C_ν belongs to capture, the second one to escape. All the complexity of the capture-escape processes is condensed here in one parameter τ_ν per particle sort, that we name capture time. Similar expressions are used in recent device simulations [18, 21]. We show in Appendix A that the above expressions follow from the microscopic models under rather general assumptions. We give also evidence that the capture times are independent of F_ν and they are also independent of injection current I. These properties are important for understanding the impact of a finite capture time on the voltage-current characteristics. Electrons and holes generally have different capture times. They are not only difficult to calculate but they are also difficult to measure. In literature, values between some fs and several ten ps have been reported for QWs similar to those in our devices [2, 16, 12, 18]. In view of this uncertainness we choose identical capture times, $\tau_{\mathsf{e}} = \tau_{\mathsf{h}} = \tau$. This is particularly justified in our material where the hole capture time has only a marginal influence, see the discussion after formula (17). We compare only two characteristic cases, $\tau \to 0$ and $\tau = 1$ ps which lead to good equivalence with measured devices, representing extremely fast capture and a moderately slow capture, respectively. In first case, the parentheses in (4) must vanish in order to keep the C_μ value finite. Free and bound Fermi levels are equal to each other in this case. In the other case, positive values of C_ν require $F_e > F_{be}$ and

F_h<F_{bh} as sketched in Fig. 1. Thus, the Fermi voltage $U_{\mathsf{QW}} = (F_{\mathsf{e}} - F_{\mathsf{h}})/e$ of free electron-hole pairs in the QW, which is the main contribution to the total voltage U across the device, depends on τ.

The recombination rate of free states in (1) is

$$R = \left(\frac{1}{(p+n_i)\tau_n + (n+n_i)\tau_p} + B + \tilde{C}_n n + \tilde{C}_p p \right) (np - n_0 p_0), \tag{6}$$

where $\tilde{C}_\nu$ denotes Auger coefficients in contrast to the net capture rates C_ν. Assuming midgap recombination centers, the intrinsic concentration $n_i = \sqrt{N_c N_v \exp(-E_g/kT)}$ is used in the denominator of the Shockley-Read-Hall contribution (first term). Using the product $n_0 p_0$ of equilibrium densities instead of the common n_i^2 ensures vanishing recombination in the highly doped regions close to Ohmic contacts. Parameter values are given in Section 3. The recombination rate R_{b} of bound particles is found using a similar expression and the stimulated recombination rate is found using the following equation

$$R_{\mathsf{stim}} = \frac{\Gamma g(n_{\mathsf{b}}, p_{\mathsf{b}}) \bar{P}}{\hbar \omega d w}. \tag{7}$$

The confinement factor Γ is determined from the fundamental vertical mode $\phi(y)$ obtained by solving the standard Helmholz equation for the unbiased vertical waveguide. This procedure is standard and needs not to be detailed here. The gain function is

$$g(n_{\mathsf{b}}, p_{\mathsf{b}}) = g' \ln\left(\sqrt{n_{\mathsf{b}} p_{\mathsf{b}}}/n_{\mathsf{btr}}\right) \tag{8}$$

with parameters obtained by fitting to kp8 calculations (see subsequent Section 3). The required carrier densities of bound particles to reach threshold are rather high (>1e18 cm^{-3}) so that the electrons are degenerate and Boltzmann expressions as in equation (5) are no more valid. We use instead an expression introduced by [22]

$$\begin{aligned} n_{\mathsf{b}} &= n_c F_{\mathsf{U}}(\eta_{\mathsf{be}}), \quad \eta_{\mathsf{be}} = \frac{F_{\mathsf{be}} - E_{\mathsf{be}}}{kT}, \\ p_{\mathsf{b}} &= n_v F_{\mathsf{U}}(\eta_{\mathsf{bh}}), \quad \eta_{\mathsf{bh}} = \frac{E_{\mathsf{bh}} - F_{\mathsf{bh}}}{kT}, \\ &\text{with } F_{\mathsf{U}}(\xi) = \frac{(0.307 \ln[1+\exp(\xi)]+1)^2 - 1}{0.614}. \end{aligned} \tag{9}$$

Although the original relations are approximations of the Fermi integral $F_{1/2}(\eta)$ [22], they are also a reasonable fit for the bound states in our structures (see subsequent Section 3.)

The optical losses

$$\alpha = \alpha_0 + \alpha_R + \alpha_{\mathsf{fc}}, \qquad \alpha_R = \frac{1}{L} \ln\left(\frac{1}{\sqrt{R_0 R_L}}\right) \tag{10}$$

contain a constant background loss, the outcoupling loss, and free carrier absorption. Two photon absorption is disregarded because it is negligible close to threshold. The free carrier absorption is

$$\alpha_{\mathsf{fc}} = \Gamma(f_{\mathsf{fn}} n_b + f_{\mathsf{fp}} p_{\mathsf{b}}) + \int [f_{\mathsf{fn}} n(y) + f_{\mathsf{fp}} p(y)] \phi^2(y) \, \mathrm{d}y, \tag{11}$$

with coefficients $f_{\mathsf{f}\nu}$ that may vary among the layers. The second term depends on the vertical distributions $n(y)$ and $p(y)$ of free carriers determined by solving the outside transport problem in the next subsection. The $\bar{P}$ in the stimulated recombination (7) is the longitudinally averaged power in the waveguide. The output power is

$$P = \frac{\alpha_R L}{1+\xi} \bar{P}; \qquad \text{with } \xi = \frac{1-R_L}{1-R_0} \sqrt{\frac{R_0}{R_L}}. \tag{12}$$

.

2.2 High-Injection Drift-Diffusion Model

The stationary flow of free carriers in the p- and n-regions is described by the well-established drift-diffusion equations (see e.g. [9])

$$\partial_y j_\nu = -e_\nu R \quad \text{and} \quad \mu_\nu n_\nu \partial_y F_\nu = j_\nu \tag{13}$$

with boundary conditions described below. The notation here is $e_\mathsf{e} = -e, n_\mathsf{e} = n$ and $e_\mathsf{h} = e, n_\mathsf{h} = p$. The particle densities are related to the quasi Fermi energies also by the Unger fit $F_\mathsf{U}(\eta)$ to the Fermi integral as shown in equation (9) for bound densities in the QW. The band edges $E_\nu = E_{c/v}(y) - e\varphi(y)$ depend on position for two reasons. First, the band edges $E_{c/v}$ of the materials vary from layer to layer. Second, the electrostatic potential $\varphi(y)$ varies, too. It solves the Poisson equation and depends non-locally on the whole charge distribution. This prevents a separate treatment of the outer regions and the QW. In addition, a semiconductor laser at threshold and above operates in the high-injection regime. As a result, the density of mobile charges is high so that the Debye screening length falls below the thicknesses of the layers. As a consequence, charge neutrality occurs in a large portion of each layer. In these parts, the potential φ is locally determined, the layers are decoupled from each other. This situation is accounted for by the neutrality approximation [10, 15]

$$N_c F_\mathsf{U}\left(\frac{F - E_g}{k_B T} - \eta_\mathsf{h}\right) - N_v F_\mathsf{U}\left(\eta_\mathsf{h}\right) = N_D - N_A, \tag{14}$$

where $F = F_\mathsf{e} - F_\mathsf{h}$ is the Fermi energy of electron-hole pairs and $\eta_\mathsf{h} = (E_v - e\phi - F_\mathsf{h})/kT$. The left hand side is a monotonously decreasing function of η_h. Thus, this equation has always a unique solution easily found with Newton's iteration. For given material parameters, the solution depends only on F. Furthermore, the total current density $j_\mathsf{tot} = j_\mathsf{e} + j_\mathsf{h}$ is a constant along the device. Therefore, it is useful to transform the drift diffusion system (13) into equations for F and one current component, e.g., for the electrons. The transformed equations are

$$\begin{aligned} &\partial_y F = \frac{j_n}{\mu_\mathsf{e} n_\mathsf{e}(F)} - \frac{j_\mathsf{tot} - j_n}{\mu_\mathsf{h} n_\mathsf{h}(F)}, \;\; \partial_y j_n = -e_\mathsf{e} R(F), \\ &F(y_\mathsf{QW}) = F_\mathsf{QW}, \quad F(y_\mathsf{c}) = 0, \end{aligned} \tag{15}$$

where F_QW is the difference $F_e - F_h$ of the Fermi levels of free particles in the quantum well as used in Eq. (5). They hold on both sides of the QW independent of each other. A corresponding equation for the p current is obtained by just inserting $j_n = j_\mathsf{tot} - j_p$. At heterojunctions, F and j_n are continuous. The boundary condition at y_c is the equilibrium condition for an Ohmic contact. The other boundary condition is continuity of the Fermi levels of free particles at the boundary to the QW.

These equations together with the QW balances (1), the neutrality and threshold conditions (2) and subsequent formula for the coefficients determine completely the bound Fermi levels in the QW, and the free Fermi levels, current and carrier densities in the whole device with contact width w and length L for given injection current $I = wLj_\mathsf{tot}$. Note that the solutions of (15) also define the current densities entering the QW via the balance equations (1):

$$\begin{aligned} &\text{n-side: } j_\mathsf{eInject} = j_n(y_\mathsf{QW}), \;\; j_\mathsf{hLeak} = j_p(y_\mathsf{QW}) \\ &\text{p-side: } j_\mathsf{hInject} = j_p(y_\mathsf{QW}), \;\; j_\mathsf{eLeak} = j_n(y_\mathsf{QW}). \end{aligned} \tag{16}$$

We solve the set of equations with an in-house MATLAB code HILM using adaptive grids on both sides of the QW.

Table 1. Global parameters

		Temperature T (K)		
Parameter	Unit	298	248	218
wavelength:				
λ	10^{-9} m	970	955	940
Recombination (6):				
$\tau_{\mathrm{n}} = \tau_{\mathrm{p}}$	10^{-9} s	2.8	2.8	2.8
B	10^{-16} m^{3}s^{-1}	2.1	2.8	4.1
$\tilde{C}_{\mathrm{n}} = \tilde{C}_{\mathrm{p}}$	10^{-43} m^{6}s^{-1}	10	4.6	1.4
Free carrier absorption (11):				
f_{fn}	10^{-22} m^2	4	3.3	2.7
f_{fp}	10^{-22} m^2	12	8.3	5.3
gain (8):				
g'	10^5 m^{-1}	2.5	2.5	2.5
n_{btr}	10^{24} m^{-3}	1.4	1.1	0.85

3 Laser structures and simulation parameters

In order to study the impact of finite capture time on differential resistance, five structures differing in the Al content were investigated. All vertical structures use a single quantum well (QW) emitting at a wavelength of approximately $\lambda = 970$ nm at room temperature. Those structures are described in detail in [6] and distinguished by the Al content of the optical confinement layers (mol fraction, $Al_xGa_{1-x}As$ $x = [0.075, 0.1, 0.125, 0.15, 0.175]$) which determines the barrier height for each structure. As in [6], those vertical designs were grown using MOVPE (metal-organic vapor phase epitaxy) techniques and processed into single emitters with resonator lengths $L = 4$ mm and contact stripe widths $w = 100$ μm. Afterwards, the bars were coated with 98 % back facet and 2% front facet reflectivity and then single chips were mounted on CuW heatsinks with AuSn solder. They were tested in pulsed mode (pulse length 1.2 ms, repetition frequency 10 Hz) at three different temperatures, $T = [218, 248, 298]$ K. The detailed measurement results have been presented in [6] and in this paper, only summarized results are presented.

Most of the parameters entering the simulation were obtained in a similar manner as described in [13]. The values for the differential gain g', the transparency concentration n_{btr}, the effective densities of states n_c and n_v of the QWs and the coefficient B of radiative recombination were determined from the results of a quantum–mechanical **kp**8 calculation [23]. This is exemplified in Figure 2 for the case $x = 0.15$ and $T = 298$ K. Equally good agreement is as obtained for the other temperatures (not shown). The lifetimes due to Shockley–Read–Hall recombination (2.8 ns, equal for electrons and holes, see Table 1, were used as parameters to fit the threshold.

We assume always the same band gap of the QW which is adapted to the average of the measured lasing wavelength for the different structures for each temperature. The most important material parameter used in simulation at the three temperatures $T = [218, 248, 298]$ K are presented in the table.

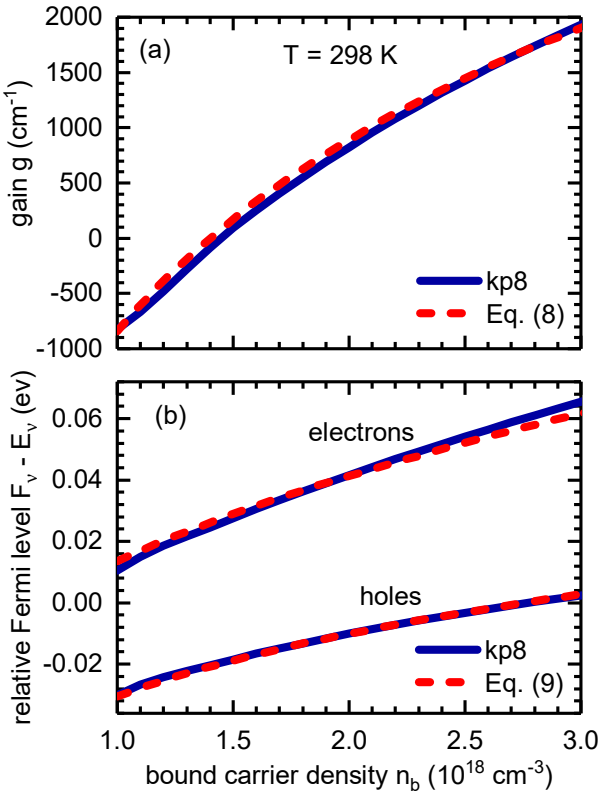

Figure 2: Comparison of the results of **kp**8 calculations to (a) the gain formula (8) and (b) the Unger fit (9) for the Fermi levels of bound particles.

4 Results

The two main aims of this section are (i) to reveal by simulations the impact of the capture time τ on the characteristics of a SQW laser, in particular on its differential resistance slightly above threshold and (ii) to verify these theoretical results by comparison with measurements. For these purposes, we compare simulations for the two cases of an infinitely fast capture, $\tau = 0$, and a moderately slow capture, $\tau = 1$ ps. In subsections 4.1 and 4.2 we look in detail on the dependencies on injection current, temperature, and barrier height, respectively. In all cases the scenarios $\tau = 1$ ps are much closer to experiment than infinitely fast capture. In subsection 4.3, all differential resistances at $I = 2$ A calculated for different temperatures and barrier heights are compared to experiment. Although a certain variation of the capture time across real samples and temperatures can be expected, the representative case $\tau = 1$ ps reproduces the overall experimental trends well.

4.1 Dependence on injection current

In this section, the impact of capture time on power-current and voltage-current characteristics will be investigated for the exemplary case $x = 0.15$ and $T = 298$ K. The calculated UI curve for slow capture in Fig. 3(a) is up to 100 mV above that for fast capture. Furthermore, it exhibits curvature or saturation, whereas the UI for fast capture is straight. These observations are more clearly illustrated in panel (b) that shows the differential resistances $R_d = \mathrm{d}U/\mathrm{d}I$. The constant R_d for $\tau = 0$ is just the summed bulk resistance of the p- and n-layers. Moving to $\tau = 1$ ps causes a current dependent, hyperbolic shaped shift of R_d (red line). This shift has to be due to capture related effects in the

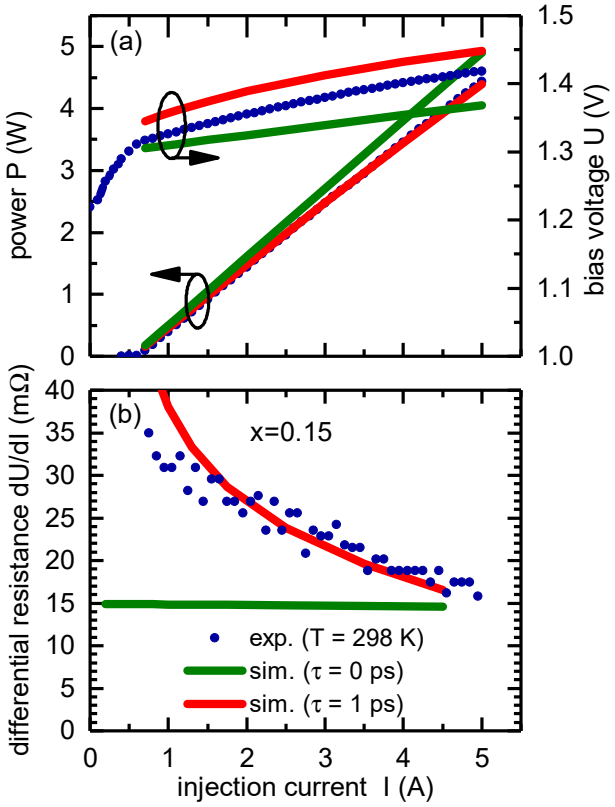

Figure 3: a) Optical output power (left axis) and bias voltage (right axis) versus injection current at $T = 298$ K for the structure with x=0.15 Al content in the optical confinement layers. Experiment (blue), fast capture (green) and slow capture (red). b) Differential resistance of the same structure as in (a) versus injection current at $T = 298$ K for τ = 0 (fast capture) and $\tau = 1$ ps (slow capture), green and red curve, respectively and measurement (blue).

quantum well because the bulk resistance does not change.

In order to better understand these effects, we derive an analytical approximation for the UI characteristics from the balance equations (1). We assume $I = j_{\text{elnject}} wL$, i.e. neglect leakage currents and recombination of free carriers in the QW. Multiplying (1) with wL and resolving the C_ν for F_ν yields

$$\begin{aligned} F_\nu &= F_{\text{b}\nu} \pm kT \ln\left[1 + \frac{\tau_\nu}{Q_\nu} I\right] \quad \text{with} \\ Q_\nu &= edwLn_c \exp\left[\pm \frac{F_{\text{b}\nu} - E_\nu}{kT}\right], \end{aligned} \tag{17}$$

where the upper sign belongs to electrons and the lower one to holes. Since the laser condition pins $F_{\text{b}\nu}$, the quantities Q_ν do not vary with I. For $\tau_\nu = 0$, the Fermi levels of free particles are pinned to those of the bound particles, too. Hence, the Fermi voltage $(F_{\text{e}} - F_{\text{h}})/e$ does not contribute to the differential resistance. With positive capture times, this Fermi voltage leads to an additional contribution that varies logarithmically with I. This fact explains the observed bending of the uppermost UI curve and it yields a hyperbolic variation of its derivative R_d with current I. In our example we have $Q_{\text{e}}/\tau_{\text{e}} = 220$ mA and $Q_{\text{h}}/\tau_{\text{h}} = 7.6$ A. Hence, the additional voltage is mainly due to electrons. It varies from about 30 mV at threshold $I_{\text{th}} \approx 0.6$ A to about 80 mV at $I = 5$ A in agreement with the

numerical curve (red curve) in Fig. 3(a). It would triple for a fictive larger $I = 100$ A, introducing an extra 24 W heat source in addition to the 15 W heating by the bulk resistance. By these figures, the capture time becomes a possibly important parameter for high-power quantum-well lasers. Since our model does not include effects of extremely high injection like two-photon absorption and temperature rise, we will not consider currents above 5 A. We assess instead, whether the assumed $\tau = 1$ ps is realistic in this range of operation.

To this purpose, we compare now with measurements. Detailed measurement conditions are explained in Sec. (3). The bending of the UI curve for $\tau = 1$ ps and, consequently, the R_dI curve reproduce well the measured data, as shown in Fig. 3. In contrast, the $\tau = 0$ curves disagree. We conclude that the measured non-trivial dependence of R_d on I can be obtained by working with a finite capture time of the order of one ps. However, the simulation result for 1 ps shows approx. 30 mV higher voltage compared to the measured voltage (blue circle). This difference could be reduced by choosing a much smaller capture time. But in result, the good agreement of the R_d curves would disappear. So we keep 1 ps in what follows and accept the too large calculated voltages which are perhaps due to our method of choosing the bulk band gap energy of the QW in such a way, that the difference of the first confined states (subband edges) of electrons and holes is equal to the lasing photon energy. This assumption exaggerates the threshold voltage because in a FP laser the spectral gain peak determines the lasing wavelength.

In what follows, we shall compare simulation and measurement for different temperatures and for devices with five different aluminium contents x in the optical confinement layers. It is impossible to present the whole characteristics for so many cases. Instead, we consider the differential resistance $\frac{dU}{dI}$ at 2 A above threshold and its deviation from the bulk resistance as an indicator of the discussed capture effects. In the singular case considered so far, both the measured and the calculated R_d in Fig. 3b are nearly twice as large as the bulk resistance at this current. A similar agreement for different temperatures and different structures will be shown here and is a strong evidence for the impact of the capture time on the real devices.

Before continuing, we complete this subsection with considering the PI curves in Fig. 3. Compared to the straight line (green) for $\tau = 0$, the curve for $\tau = 1$ ps (red) exhibits a beginning saturation, again in agreement with the experiment. This behaviour is also in qualitative agreement with results of reference [1]. In our case, the finite capture time τ causes bending of the PI curve by raising the leakage current. To understand this effect, it is useful to ask how the current required for a given power depends on τ. According to balance (1), the total current $I = I_{\text{stim}} + I_{\text{R}} + I_{\text{Leak}}$ is composed of contributions feeding the stimulated recombination, feeding all other recombinations in the QW, and the sum of leakage currents, respectively (see also Fig. 1). I_{stim} is fixed by the given power. I_{R} is not affected by τ and it is clamped by the threshold condition (2), here at about 600 mA. Leakage out of the QW is proportional to the densities n_ν of minority carriers outside the QW (Eq. (13)), which are proportional to the respective free carrier densities (5) in the QW, which in turn must rise with τ to keep the net capture rates (4) unchanged. Thus, I_{Leak} at a given power grows with increasing τ shifting I to larger values. This shift is small at threshold (22 mA in our example) and increases slightly down-bended to 350 mA at $P = 4$ W.

4.2 Dependence on temperature and on barrier height

The dependence of differential resistance on temperature is demonstrated in Fig. 4a looking at three different temperatures $T = [218, 248, 298]$ K, still for the structure with $x = 0.15$. To reduce the uncertainties in view of the large scatter of the experimental R_d values in Fig. 3b, a mean resistance is

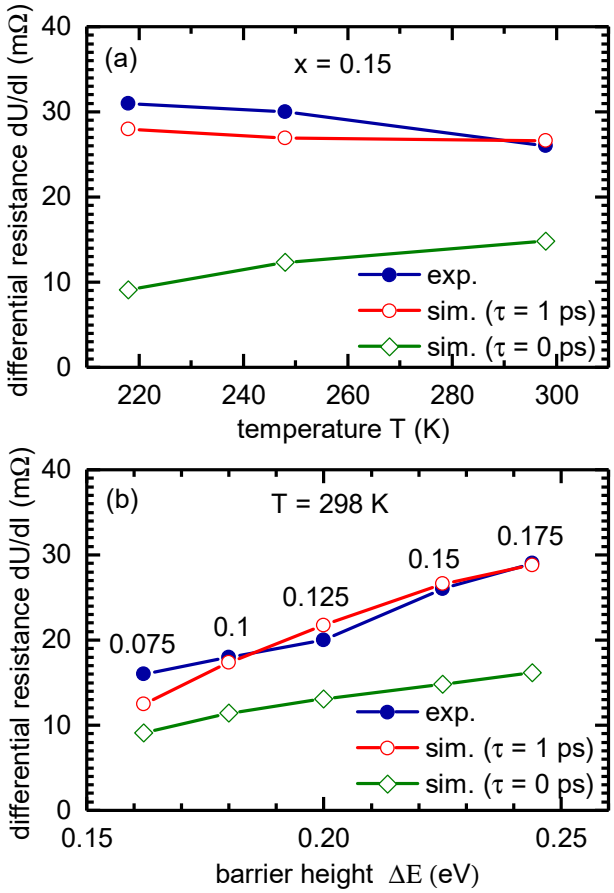

Figure 4: (a) Calculated and measured differential resistance at 2 A for the structure with Al content, $x = 0.15$ in the optical confinement layers versus temperature at $T = [218, 248, 298]$ K and $I = 2$ A. Measured (blue), simulated (slow capture - red and fast capture - green) (b) Calculated and measured differential resistance versus barrier height (difference between the gap energy in the optical confinement layers and first confined electron state) at $T = 298$ K and $I = 2$ A for structures with different Al content, x.

always calculated by taking the linear slope between the voltages at $I_{\rm th} + 0.5$ A and $I_{\rm th} + 2.5$ A. The simulation results with $\tau = 1$ ps deviate from the experiment only slightly. At room temperature, the deviation is much smaller but increases towards lower temperature as the capture time is assumed to be constant (1 ps) for all temperatures. The full resistance for $\tau = 1$ ps of simulation and experiment both decrease with temperature. The simulation result with $\tau = 0$ ps follows the opposite trend, it decreases with decreasing temperature due to increasing mobility in contrast to the measurement. This is due to not considering the capture-escape process in the simulation. These results show that the finite capture time has a strong impact on the resistance, which more than doubles at low temperatures compared to zero capture time. These facts support the idea that also the measured excess resistance is mainly due to a slow capture time.

Now let us consider the dependency of differential resistance R_d on barrier height. All five structures have been considered for this analysis and simulations are performed with slow and fast capture at T= 298 K. The results are shown in Fig. 4b versus the barrier height, which is assumed to have a dominant influence [8]. As in [8], the barrier height ΔE is determined by the energy difference between the QW confined electron state and the band edge of the optical confinement layers. The hole barrier is of minor influence because holes contribute only marginally to the excess voltage, see the discussion

after formula (17). R_d increases with increasing ΔE for fast and slow capture, in both cases. However, the increment is much faster in case of slow capture (marked in red). This surplus increment $\Delta R_d^{\text{capture}}$ in excess of the bulk resistivity can be understood in the context of formula (17). The most relevant quantity Q_{e} depends exponentially on $F_{be} - E_{\mathsf{e}} = (F_{be} - E_{be}) - (E_{\mathsf{e}} - E_{be})$. The first bracket does not depend on the barrier height, $\Delta E = E_{\mathsf{e}} - E_{be}$ due to threshold condition. The second bracket is the barrier height itself. Hence, Q_{e} decreases with ΔE and the excess $\Delta R_d^{capture} \sim (Q_{\mathsf{e}}/\tau + I)^{-1}$ increases as long as Q_{e}/τ is larger or comparable with I. The measured resistance shows just this tendency. The small discrepancy between measurement and simulation for finite capture time is possibly due to factors not contained in the discussed approximation.

4.3 Dependence on relative barrier height $\Delta E/kT$

As seen in our earlier experimental study [6, 8], the differential resistance R_{d} close to threshold is a strong function of the relative barrier height $\Delta E/kT$. For better comparison, we have re-evaluated these measurements of the five vertical structures with different x, each one at three different heat sink temperatures. Results are plotted in panel (a) of Fig. 5. The trends of [6] are reproduced. In all samples, the measured differential resistance is up to three times larger than the bulk resistance, which is estimated from the mobilities, doping concentrations, and thicknesses of all layers. This excess resistance contains all possible contributions from the QW, from interfaces and from the contacts.

The corresponding simulation results depicted in panel (b) do not contain contributions from either heterointerfaces or contacts. Note that the curves for $\tau = 0$ agree quite well with the bulk resistance curves in panel (a). The negligibly small deviations are due to leakage of minority carriers from the QW taken into account in panel (b) but not in panel (a). The two curves of the same colour in panel (b) differ by the excess resistance caused by the assumed finite capture time $\tau = 1$ ps. When effective barrier height, $\Delta E/kT > 12$, R_s approaches to approx 30 mΩ. Since the capture-escape-related excess resistances of all five structures coincide quite well in magnitude and slope with the measured ones, we conclude that (i) the measured excess resistance is most likely capture-escape related and (ii) the experimental capture times are of the order of 1 ps or not much less. The deviation between simulation and experiment results mainly from the following factors. First, the capture time is assumed to be independent of barrier height (considered to be $\tau = 1$ ps for all structures and temperatures). Second, no substrate and contact resistances are considered in simulation but must exist in the experiment. Third, the measurement process may induce errors. Despite these limitations, simulation results match quite well with the experiment.

5 Conclusion

We have demonstrated the presence of significant excess resistance related to capture-escape processes in high-power quantum-well lasers. It acts in addition to and is larger than the Ohmic resistance of the bulk parts of the device. High power requires strong pumping of the lowest subbands of the quantum well, which feed the stimulated emission. These confined subbands do not have a direct connection to the device contacts. Thus, the injected charge carriers must subsequently be captured into these subbands. High capture rates in connection with limited capture probabilities require a distinct difference between the bulk and subband Fermi levels, which appears as an excess voltage at the contacts and is the source for the excess resistance.

The study presented here has transformed this narration into a quantitative theory. A drift-diffusion

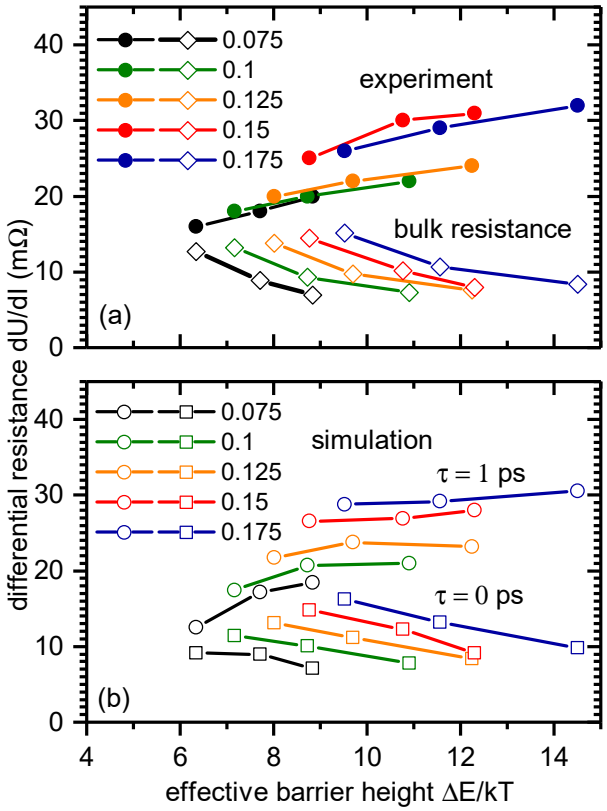

Figure 5: Differential resistances at $I = 2$ A of structures with different Al contents (legend) versus effective barrier height. (a) Closed circles: measured, open diamonds: bulk layer resistance. (b) Open circles: simulation with $\tau = 1$ ps (slow capture), open squares: simulation with $\tau = 0$ (fast capture).

description in quasi neutrality approximation allows us to precisely calculate the current flow outside the quantum well. The model for the net capture-escape rate has already been used by other authors with heuristic reasoning. It is derived here under rather general conditions, assuming internal thermalization of confined as well as unconfined particles with different Fermi energies. As a simplifying assumption, the model contains only one capture time for each particle sort as a free parameter.

On this basis, a detailed analysis was presented to quantify the excess series resistance and to understand its dependence on device parameters and temperature. Five vertical structures with different Al content from [6] were simulated at three different heat sink temperatures, $T = [218, 248, 298]$ K. Since the capture times of our structures are unknown, we have done calculations with $\tau = 0$ and 1 ps for electrons as well as holes and compared the results to measurements. The $\tau = 0$ results reproduce well the bulk-layer Ohmic resistances. The $\tau = 1$ ps excess resistances vary from 1 mΩ up to 30 mΩ and are in good agreement with experiment. In particular, the results agree with the measured and so far unexplained increase of the series resistance with lower heat sink temperature. We therefore conclude that the excess resistances in the experimental structures are mainly due to capture-escape processes as described by our model and that these are larger than bulk layer and packaging resistance and so are a significant limit to conversion efficiency. Slow capture rates can also cause additional limit to output power due to enhanced losses in the optical confinement layers. Keeping the electron capture time as short as possible is required to diminish these unfavorable effects. Hader at al. have pointed out ”that the capture can be made faster by using structures with a larger ratio of well- to barriermaterial” [12] but systematic experimental or theoretical studies of this subject are missing yet.

A substantiation of the capture-escape rate (4)

We consider electron capture as representative. The index e is suppressed for clarity. k_f and k_b denote all quantum numbers of free and bound states, respectively. The respective occupation probabilities are

$$\begin{aligned} f(k_f) &= \left(\exp\left[\frac{E(k_f)-F_f}{kT}\right]+1\right)^{-1} \quad \text{and} \\ f(k_\mathsf{b}) &= \left(\exp\left[\frac{E(k_\mathsf{b})-F_\mathsf{b}}{kT}\right]+1\right)^{-1}. \end{aligned} \tag{18}$$

Capture of an electron requires that excess energy and transverse momentum are transferred to other elementary excitations. Let q denote the quantum numbers of the involved elementary excitations. In the context of the golden rule of quantum mechanics, the total capture-escape rate is written as [2, 11]

$$\begin{aligned} C = &\sum_{k_f,k_\mathsf{b},q} M^2(k_f,k_\mathsf{b},q)\delta(E(k_f)-E(k_\mathsf{b})-\Omega(q))\times \\ &\times\left[f(k_f)(1-f(k_\mathsf{b})p^+(q)-(1-f(k_f))f(k_\mathsf{b})p^-(q)\right]. \end{aligned} \tag{19}$$

M^2: quantum mechanical matrix elements of the transitions (positive). $p^\pm(q)$: probability for creation / annihilation of the energy absorbing elementary excitation q. The most important excitations are phonons and electron-electron scattering in the bound subbands. With phonons of temperature T, one has $p^+(q)=1+f_B(q)$ and $p^-(q)=f_B(q)$ with the Bose distribution $f_B(q)=1/(\exp(\Omega(q))-1)$. The contribution due to electron scattering from k_i to k_f has $p^+=f(k_i)(1-f(k_f))$ and $p^-=f(k_f)(1-f(k_i))$. Here, k_i and k_f must belong to the same electron type, either free or bound.

Simple calculations yield

$$\frac{p^-(q)}{p^+(q)} = \exp\left(-\frac{\Omega(q)}{kT}\right) \tag{20}$$

in all cases. Thus, taking the first term out of the occupation factor in (19) and keeping in mind energy conservation, one arrives at

$$C = \left[1-e^{\frac{F_\mathsf{b}-F_f}{kT}}\right]\sum_{k_f,k_\mathsf{b}} \widetilde{M^2}(k_f,k_\mathsf{b})f(k_f)(1-f(k_\mathsf{b})) \tag{21}$$

with

$$\begin{aligned} \widetilde{M^2}(k_f,k_\mathsf{b}) = &\sum_q M^2(k_f,k_\mathsf{b},q)\times \\ &\times\delta(E(k_f)-E(k_\mathsf{b})-\Omega(q))p^+(q). \end{aligned} \tag{22}$$

The only approximation so far is assuming the bound and free particles as well as the phonons being in internal quasi equilibria with a common temperature T. Under this condition, the square-bracket occupation factor in front of a non-negative rest is a general property of C. It ensures net capture ($C>0$), net escape ($C<0$), and balance ($C=0$) in cases $F_f<F_\mathsf{b}, F_f<F_\mathsf{b}$, and $F_f=F_\mathsf{b}$, respectively.

Now we further adapt (21) to the situation of the present paper. Small free particle densities enable the Boltzmann approximation $f(k_f) = \exp([F_f - E(k_f)]/kT)$. This yields

$$C = \left[1 - e^{\frac{F_\mathrm{b} - F_f}{kT}}\right] \frac{n}{\tau} \quad \text{with} \tag{23}$$
$$\frac{1}{\tau} = \sum_{k_f, k_\mathrm{b}} \widetilde{M^2}(k_f, k_\mathrm{b}) \exp\left(\frac{E_f^0 - E(k_f)}{kT}\right) (1 - f(k_\mathrm{b}))$$

where E_f^0 is the minimum of the free electron band.

It is important to note that only scattering between free electrons can cause a dependence of the capture time τ on F_f via the factor $p^+(q)$. Thus, τ is independent of F_f as long as the free electron concentration in the QW remains small. Since this is the case in a well designed laser and F_b is clamped by the threshold condition, we expect that τ is nearly independent of the injection current I above threshold. Of course, it changes when changing the device structure and the temperature.

References

[1] L. Borruel, J. Arias, B. Romero, and I. Esquivias. Incorporation of carrier capture and escape processes into a self-consistent cw model for quantum well lasers. *Microelectronics journal*, 34(5-8):675–677, 2003.

[2] J. Brum, T. Weil, J. Nagle, and B. Vinter. Calculation of carrier capture time of a quantum well in graded-index separate-confinement heterostructures. *Physical Review B*, 34(4):2381, 1986.

[3] P. Crump, M. Grimshaw, J. Wang, W. Dong, S. Zhang, S. Das, J. Farmer, M. DeVito, L. S. Meng, and J. K. Brasseur. 85% power conversion efficiency 975-nm broad area diode lasers at $-50°$c, 76% at $10°$c. In *2006 Conference on Lasers and Electro-Optics and 2006 Quantum Electronics and Laser Science Conference*, pages 1–2. IEEE, 2006.

[4] I. Esquivias, S. Weisser, B. Romero, J. Ralston, and J. Rosenzweig. Carrier dynamics and microwave characteristics of gaas-based quantum-well lasers. *IEEE Journal of Quantum electronics*, 35(4):635–646, 1999.

[5] B. Faraji, D. Pulfrey, and L. Chrostowski. Small-signal modeling of the transistor laser including the quantum capture and escape lifetimes. *Applied Physics Letters*, 93(10):103509, 2008.

[6] C. Frevert, P. Crump, F. Bugge, S. Knigge, and G. Erbert. The impact of low al-content waveguides on power and efficiency of 9xx nm diode lasers between 200 and 300 k. *Semiconductor Science and Technology*, 31(2):025003, 2016.

[7] C. Frevert, P. Crump, H. Wenzel, S. Knigge, F. Bugge, and G. Erbert. Efficiency optimization of high power diode lasers at low temperatures. In *2013 Conference on Lasers & Electro-Optics Europe & International Quantum Electronics Conference CLEO EUROPE/IQEC*, pages 1–1. IEEE, 2013.

[8] C. Frevert, S. Knigge, G. Erbert, F. Bugge, and P. Crump. Influence of quantum well barrier height on series resistance in gaas-based broad area diode lasers. In *2018 IEEE International Semiconductor Laser Conference (ISLC)*, pages 1–2. IEEE, 2018.

[9] H. Gajewski. On existence, uniqueness and asymptotic behavior of solutions of the basic equations for carrier transport in semiconductors. *ZAMM-Journal of Applied Mathematics and Mechanics/Zeitschrift für Angewandte Mathematik und Mechanik*, 65(2):101–108, 1985.

[10] I. Gasser, C. D. Levermore, P. A. Markowich, and C. Schmeiser. The initial time layer problem and the quasineutral limit in the semiconductor drift-diffusion model. *European Journal of Applied Mathematics*, 12(4):497–512, 2001.

[11] M. Grupen and K. Hess. Simulation of carrier transport and nonlinearities in quantum-well laser diodes. *IEEE Journal of Quantum Electronics*, 34(1):120–140, 1998.

[12] J. Hader, J. V. Moloney, and S. W. Koch. Structural dependence of carrier capture time in semiconductor quantum-well lasers. *Applied Physics Letters*, 85(3):369–371, 2004.

[13] K. Hasler, C. Frevert, P. Crump, G. Erbert, and H. Wenzel. Numerical study of high-power semiconductor lasers for operation at sub-zero temperatures. *Semiconductor Science and Technology*, 32(4):045004, 2017.

[14] H. Hillmer, T. Kuhn, A. Greiner, S. Hansmann, and H. Burkhard. The role of vertical transport and capture of electrons and holes for the transient optical response in quantum-well heterostructures. *Optical and quantum electronics*, 26(7):S691–S703, 1994.

[15] A. Jüngel and I. Violet. The quasineutral limit in the quantum drift-diffusion equations. *Asymptotic Analysis*, 53(3):139–157, 2007.

[16] B. Romero, J. Arias, I. Esquivias, and M. Cada. Simple model for calculating the ratio of the carrier capture and escape times in quantum-well lasers. *Applied Physics Letters*, 76(12):1504–1506, 2000.

[17] H. Shichijo, R. Kolbas, N. Holonyak Jr, R. Dupuis, and P. Dapkus. Carrier collection in a semiconductor quantum well. *Solid State Communications*, 27(10):1029–1032, 1978.

[18] S. Steiger, R. G. Veprek, and B. Witzigmann. Unified simulation of transport and luminescence in optoelectronic nanostructures. *Journal of computational electronics*, 7(4):509–520, 2008.

[19] J. Tang, K. Hess, N. Holonyak Jr, J. Coleman, and P. Dapkus. The dynamics of electron-hole collection in quantum well heterostructures. *Journal of Applied Physics*, 53(9):6043–6046, 1982.

[20] N. Tessler and G. Eisenstein. Modelling carrier dynamics and small-signal modulation response in quantum-well lasers. *Optical and quantum electronics*, 26(7):S767–S787, 1994.

[21] A. Tibaldi, F. Bertazzi, M. Goano, R. Michalzik, and P. Debernardi. Venus: a vertical-cavity surface-emitting laser electro-opto-thermal numerical simulator. *IEEE Journal of Selected Topics in Quantum Electronics*, 25(6):1–12, 2019.

[22] K. Unger. Reversible formulae to approximate fermi integrals. *physica status solidi (b)*, 149(2):K141–K144, 1988.

[23] H. Wenzel, G. Erbert, and P. M. Enders. Improved theory of the refractive-index change in quantum-well lasers. *IEEE J. Select. Top. Quantum Electron.*, 5(3):637–642, 1999.